Pluronics as templates for synthesis of nano hydroxyapatite: Electrospinning as a novel approach to fabricate polymer-ceramic nanofiber nanocomposites

Umesh Makwana[1]*, Suresh C. Ameta[1] and Bharat T. Thaker[2]

1. Department of Chemistry,PAHER University,Udaipur-313003 (Raj.)

2. Department of Chemistry,V.N.South Gujarat University,Surat-395007(Guj.)

Abstract:

We report the synthesis of hydroxyapatite nanoparticles by using calcium nitrate and orthophosphoric acid. Pluronics (F127) was used as a templating agent. The HA prepared was characterized using TEM, SEM, X-ray diffraction and surface area. Mainly, the concentration of surfactants and reaction temperature was varied for morphological development of nanoparticles. By template assisted method, it was possible to synthesize HA nanorods with very high aspect ratio and mesoporosity. At higher concentrations and higher temperatures Nanorods were formed and lower concentrations and lower temperatures, nanospheres were formed. X-ray diffraction showed that the crystallite size increased with decrease in surfactant concentration. Additionally, apatite layer was formed of surface of HA when immersed in simulated body fluid. Layer of apatite in the form of nano roots sprouted from the HA surface after one day immersion time. Nanofibers were fabricated using synthesized nanoparticles and with PHB as polymer matrix by using electrospinning technique.

Key words: Hydroxyapatite, Block-co-polymer-Poly (3-hydroxybutyrate), electrospinning.

1. Introduction

Significant research efforts have been made to synthesize calcium phosphate based nanobioceramics because of their potential applications in tissue engineering and biology. One of the reasons is their excellent biocompatibility with living tissues. Among the various calcium phosphates, hydroxyapatite is regarded as the most stable form of calcium phosphate among the various calcium phosphates that is being widely used in bone tissue engineering. It is similar in terms of chemical and structural composition to that of bone mineral. HA is not only bioactive but also osteoconductive, nontoxic, nonimmunogenic, and its structure is crystallographically similar to that of bone mineral. This makes HA a possible and perhaps the most appropriate bone graft material.

The stoichiometric HA has a chemical composition of $Ca_{10}(PO4)_6(OH)_2$ with a Ca/P ratio of 1.67:1. Crystallographic studies of stoichiometric HA indicate that the unit cell, a basic structural pattern of the constituent ions of HA, is a right rhombic prism that forms a simple hexagonic crystal lattice. HA is also used in many industrial applications, such as catalyst support, liquid-chromatographic columns, lighting materials, powder carriers, chemical sensors, ion conductors, retardant of cancer cells and drug delivery agent, etc [1-3]. Nevertheless, the shape, size and porosity of the HA also plays a significant role in enhancing the mechanical properties of the composite scaffolds. Several methods have been adopted to control size and shape of nanoparticles including hydrolysis[4], solid state reactions [5], precipitation[6] and surfactant templates. Surfactant templating is regarded as the most efficient method in controlling the geometries[7, 8]. Amphiphilic block copolymers (Pluronics) have been explored recently for synthesizing HA nanoparticles as they are least harmful to environment and can be used in biological applications [9].

Major drawback associated with HA is its inherent brittleness that prevents it to be used in many biological applications alone. Several methods have been adopted to reduce its brittleness either by adding inorganic particles in organic matrix or by using as such with higher macro porosities. In spite of sophisticated fabrication techniques, dispersion of inorganic constituents in organic matrix is a major challenge. One strategy for dealing with nanofabrication is to develop tissue engineered substrates by mimicking natural process which is found in nature. Natural bone is a biocomposite material composed of nanohybrid organic–inorganic components. The organic matrix is mainly Type I Collagen (Col) which provides bone its flexibility and resilience; the inorganic phase composed of mineral HA which is responsible for the stiffness and strength of bone. The organic–inorganic constituents combine together to provide a mechanical integrity in vivo.

Nanocomposites in bulk are restricted to amount of inorganic filler to be loaded in polymer matrix. Conventional nanocomposite system can synergistically perform at filler loading not more than 5wt%. Nevertheless, biological nanocomposites like bone and enamel have inorganic fillers more than 50 wt% and can attain toughness upto 20-30 GPa. Electrospinning is a novel process in which the inorganic filler in polymer nanofiber matrix is arranged in spinning direction without much agglomeration. The superfine fibers formed have diameters ranging from 10 mm down to 10 nm just by forcing a polymer solution (or polymer melt) with an electric field through a spinneret. It has been approximated that NFs with a diameter of 100 nm have a ratio

of geometrical surface area to mass of 100 m^2/g [10]. Recently, electrospun fibers have attracted great attention due to their potential applications in many fields especially in biomedical uses.

In this article, we are reporting the synthesis of shape controlled nanoparticles and fabrication of polymer/HA nanocomposite nanofibers. This was achieved using electrospinning technique which has added advantage of dispersing nanoparticles in polymer matrix without agglomeration.

2. Experimental Procedures

2.1 Starting chemicals

The starting materials used for this synthesis was calcium nitrate $Ca(NO_3)_2$ (Alfa Aeaser) and orthophosphoric acid (Labort chemicals). Pluronic F127 a block copolymer of PEO-PPO-PEO with molecular weight of 12.6 kDa was used as single surfactant from Aldrich chemicals. Ammonia solution was used as buffering medium. Poly (3-hydroxybutyrate) from sigma-aldrich was used. All the solvents were used without any further purification.

2.2 Experimental details

2.2.1 Synthesis of nanohydroxyapatite

Briefly nanoHA was synthesized as follows and is represented in a block diagram in figure 1.

The starting materials used in the present work are calcium nitrate and orthophosphoric acid for the calcium and phosphorus precursors, respectively. These reagents were used as received without any further purification. Calcium nitrate and Pluoronic F127 was dissolved in 100 gm of deionized water and vigorously stirred for about 4-5 hours until the clear micellar solution was formed. Orthophosphoric acid was used as the source for P precursors. Subsequently, the pH of the mother solution was adjusted to 11-12 by adding NH_3 solution. The ratio of calcium to phosphorous source was adjusted to 1.67:1 so as to mimic the biological apatite which has similar stiochiometric ratio in human bone. The Ca^{2+}/F127 micellar solution was slowly titrated against PO_4^- with constant stirring. The reaction temperature was maintained at 80^{o}C for 8-10 h and then aged over night at room temperature so as to allow the crystals to grow slowly. In another series, the reaction temperature was set to 7^{o}C with a jacketed reactor equipped with Julabo oil circulator bath.

The mixture was evaporated on the hotplate at 150 °C. The evaporated mass was dried on the oven at 400 °C for several hours to obtain Hap precursor powders. The precursor powders were heat-treated at different temperatures from 400 to 900 °C in a muffle furnace to obtain crystalline HA powders.

2.2.2 Fabrication of nanofibers

a) Preparation of electrospinning stock solution

Electrospinning stock solution of PHB and PHB/HA nanocomposites was prepared as follows. PHB was obtained as solution in chloroform. To fix the desired concentration, the chloroform was evaporated and obtained film was redissolved in calculated amount of chloroform required for electrospinning. Then, HA was dispersed in ethanol using ultrasonicator. PHB solution and HA suspension were mixed and stock solution was made. To avoid phase separation of mixed solvents, the composite solution was again evaporated and redissolved in only chloroform for elctrospinning at 55ºC for about 3 hours and then cooled to room temperature. This procedure was repeated for different concentration and for different filler geometry.

b) Electrospinning of nanofibers of PHB/HA

The polymer solution was filled in a 5 ml syringe equipped with a blunt steel needle of 0.9 mm inner diameter. A round copper plate covered with aluminum foil was placed 12 cm away from the needle tip as counter electrode. Electrospinning was carried out at room temperature in a vertical spinning configuration, using applied voltages in the range from 3 to 20 kV, driven by a high voltage power supply (HEINZINGER PNC, Germany) with a flow rate of 20 ml/h controlled by infusion pump. For morphological investigations, a glass slide was placed over the counter electrode as collecting substrate. The electrospun fibers were collected either directly on the aluminum foil or on grounded copper plate or on a wire mesh network to obtain a mat.

c) Preparation of simulated body fluid

Alternatively, simulated body fluid (SBF) was prepared by dissolving reagent grade chemicals of sodium chloride (NaCl), sodium hydrogen carbonate ($NaHCO_3$), potassium chloride (KCl), dipotassium hydrogen phosphate (K_2HPO_4 ·3H2O), magnesium chloride hexahydrate (MgCl2 · $6H_2O$), calcium chloride dihydrate ($CaCl_2$ ·$2H_2O$), sodium sulfate (Na_2SO_4) and tris-(hydroxymethyl) aminomethane, into distilled water and buffered to pH 7.25 at 37ºC with hydrochloric acid (HCl). Synthesized HA particles were again immersed in SBF for specific time at controlled temperature.

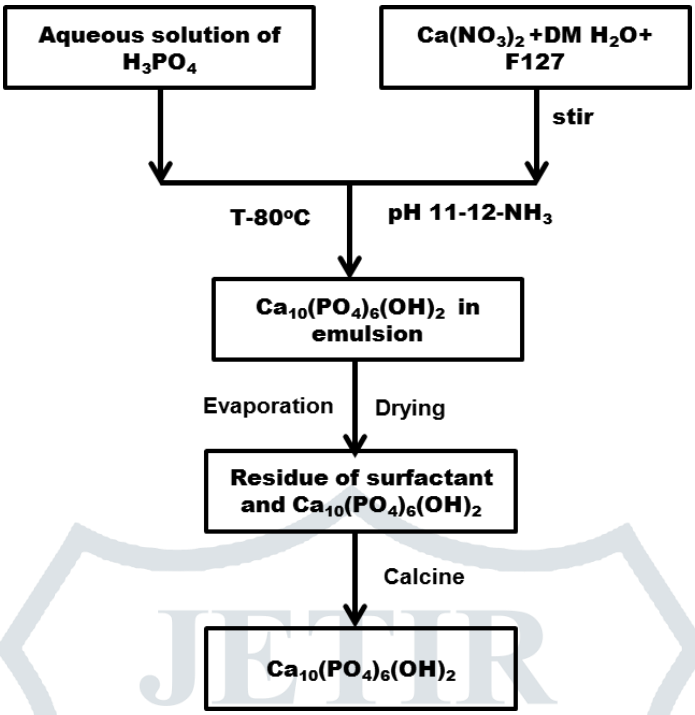

FIG. 1. Block diagram representing the synthesis of nanohydroxyapatite

2.3 Characterization

The crystalline HA powders were characterized using different analytical tools. The phase structure was determined using X-ray diffractometer (D8 Advance, Bruker KaG). Energy dispersive elemental analysis was carried out on the Inspect SEM (FEI, Netherlands). Nanoparticles for SEM and TEM (LEO 912 EFTEM) analysis were dispersed using ultrasonicator with ethanol as a medium. One drop of sonicated nanoparticle solution was suspended on a dry graphite conductive layer in case of SEM and on a copper grid in case of TEM. Later on the samples for SEM were sputter coated by gold for secondary electron imaging. Image analysis of nanoparticle was carried out using image analysis software. The specific surface area was measured following the Brunauer-Emmett-Teller (BET) method using Micrometrics and pore size distribution was determined using BJH method (Barret, Joyner and Halenda method). FTIR spectra of calcined HA was analyzed using Perkin Elmer FTIR.

3.0 Results and discussions

3.1 Morphology of nanoparticle

The morphology of as synthesized nanoparticles of HA was examined by SEM and TEM. Fig 1 shows the nanoparticle morphology of HA synthesized by varying the concentration of surfactant (F127). All the

nanoparticles synthesized at higher temperatures and at pH -11 showed rod like morphology. On an average, the smaller dimensions of nanorods were in the range of 16-70 nm and length varying in the range of 350--600 nm. Synthesized nanorods had aspect ratio of more than 10. Dimensions of the HA particles measured by image analysis software shows some differences in the nanoparticle dimensions with varying concentrations. With increasing surfactant concentration, the thickness of the nanoparticles decreased. Nevertheless, the length of the nanoparticles did not show much of the difference. Higher concentrations of F127 resulted in thinner diameter nanoparticles. According to Peiffer et al., solutions of polyethylene oxide in water cause phase separation through spinodal decomposition when temperature is raised above LCST. This phase separation pressure is dependent on molecular weight but independent of concentration [11]. As a result, nanoparticles synthesized at 80^{o}C yielded rod like morphology irrespective of change in concentration.

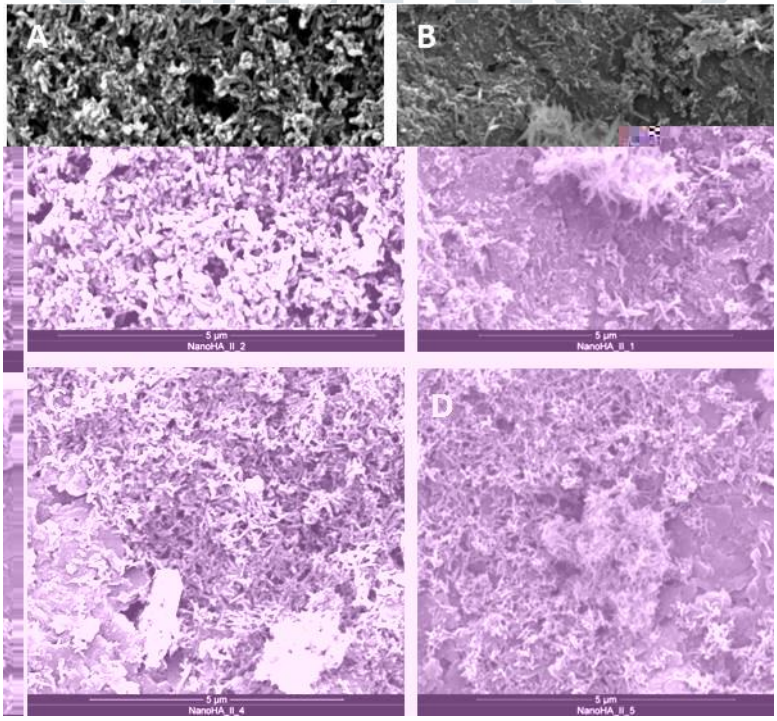

FIG. 2. Scanning electron microscope (SEM) images of as synthesized hydroxyapatite powders at different surfactant concentration and at 80^{o}C reaction temperature. The hydroxyapatite formed is rod like with aspect ratio more than 10. A) HA with 0.5wt% surfactant, B) HA with 6wt% surfactant, C) HA with 10wt% surfactant and D) HA with 15wt% surfactant.

PPO and PEO blocks at lower temperatures below 15^{o}C and at ambient pressures behaves as individual blocks. This was evidenced by Kell et al. [9] using cryogenic temperature electron microscopy. They were also able to demonstrate the existence of spherical micelles at lower temperature. Morphology of nanoparticles synthesized at 7^{o}C and with surfactant concentration similar to HA 2 yielded spherical HA nanoparticles as shown in Fig 2.

Also it was observed that the spherical nanoparticles at this temperature were not stable at ageing temperature of 25ºC. The same spherical nanoparticles were transformed into rod like ellipsoid as the temperature increased.

TABLE I: Specific surface area and crystallite size and parameters studied for HA

Sl No	Sample Code	F 127	Reaction Temperature	Crystallite size(nm)	BET
1	HA 1	0.5	80ºC	49	49
2	HA 2	6	80ºC	29	65
3	HA 3	15	80ºC	17	34
4	HA4	6	7ºC	28	45

Hence, thermodynamically stable micelles are formed at higher temperatures. However, the exact transition of spherical to rod like needs elaborate set of experiments to be carried out and stabilization of micelles at lower temperature should be accounted.

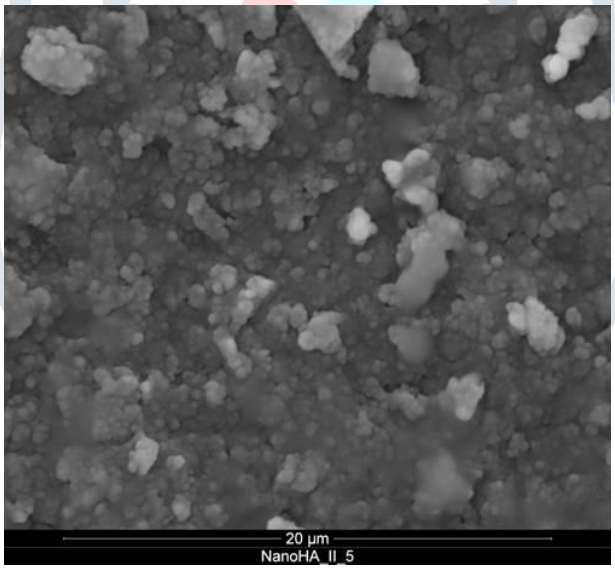

FIG. 3. SEM micrograph of as synthesized hydroxyapatite powder at 6wt% surfactant and synthesized at 7ºC. Morphology of nanoparticles are spherical with higher agglomeration rate.

Morphology of nanoparticles also changed with ageing times. Higher ageing times can allow the crystal perfection and will develop into sharp borders of defined geometry. Nanoparticles aged for 1 h showed lathe like morphology and samples aged for 24-48 h had rod like morphology.

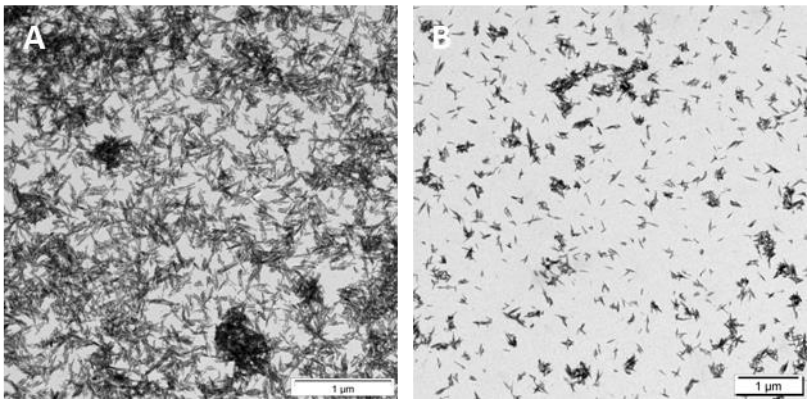

FIG. 4. TEM micrographs of morphology of HA nano rods at various ageing times A) Aged for 2 days and B) Aged for 1 hour.

3.2 BET Surface Area

The surface are of the nanoparticles were in the range as expected for typical micellar templates systems. Surface area of powders depends on the processing route and the reaction parameters. Powders with hydrothermal process can usually achieve surface area of about (31-43 m^2/g)[12] and some special techniques where controlled crystallization and freeze drying of cakes are used, it is possible to achieve as high as 300 m^2/g [13]. Pluronic systems what we used had BET surface area ranging from 34-65 m^2/g and it was higher for HA 2 powders (Fig 5).

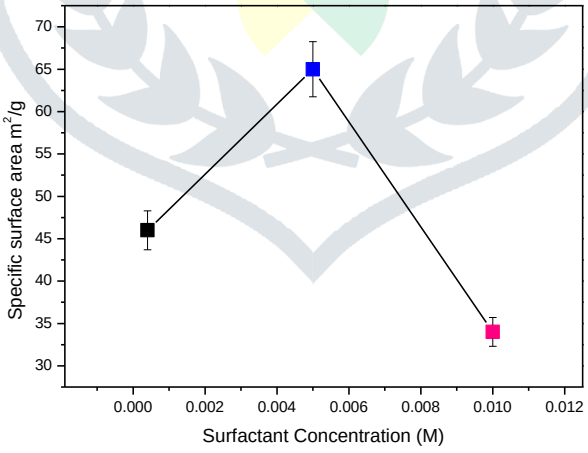

FIG. 5. Specific surface area of HA synthesized using nonionic surfactant (F127) with 0.0004, 0.005 and 0.01 M surfactant concentration.

Fig 6 shows the nitrogen adsorption desorption isotherms of HA synthesized using various surfactant concentrations. They also showed hysteresis loops, which are the characteristics of mesoporous type IV isotherms [14-16]. Hysteresis at low surfactant concentration was higher compared to that at higher concentrations and are assigned to the space between the HA.

For all the surfactant concentrations, the volume adsorbed was consistently higher at all relative pressure with pluronic systems. Contrarily, it is reported that the bulk synthesis of HA, has reduced pore volume [16]. The total pore volume was 0.65 cm^3/g for the powder prepared at lower surfactant concentrations (HA 1). Nevertheless, with increase in surfactant concentration, the total pore volume was constant at around 0.50 cm^3/g.

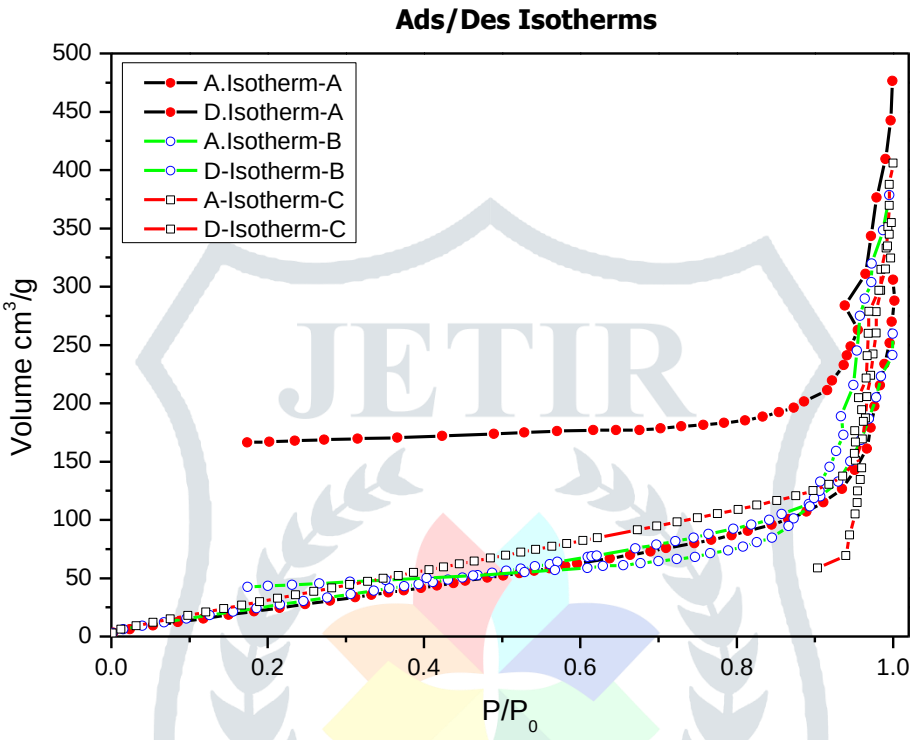

FIG. 6. Nitrogen adsorption-desorption isotherms of as synthesized HA with A) HA 1 B) HA 2 and C) HA 3 at 80°C

Even though the pore volume was higher at low surfactant concentrations, the obtained pore diameters were in the range from 20-70 nm (Fig-7). HA 3 powders showed unimodal pore size distribution. This method of HA synthesis can yield nanopores which can enhances many properties of HA other than osteoconductivity. Nanopores can be used as a drug carrier in nanomedicine and can also improve binding strength by introducing functionalized binders in the pores. Nanosized pores significantly can enhance the total surface area of the powder. It will also promote integration of the powder with other materials for improved mechanical properties.

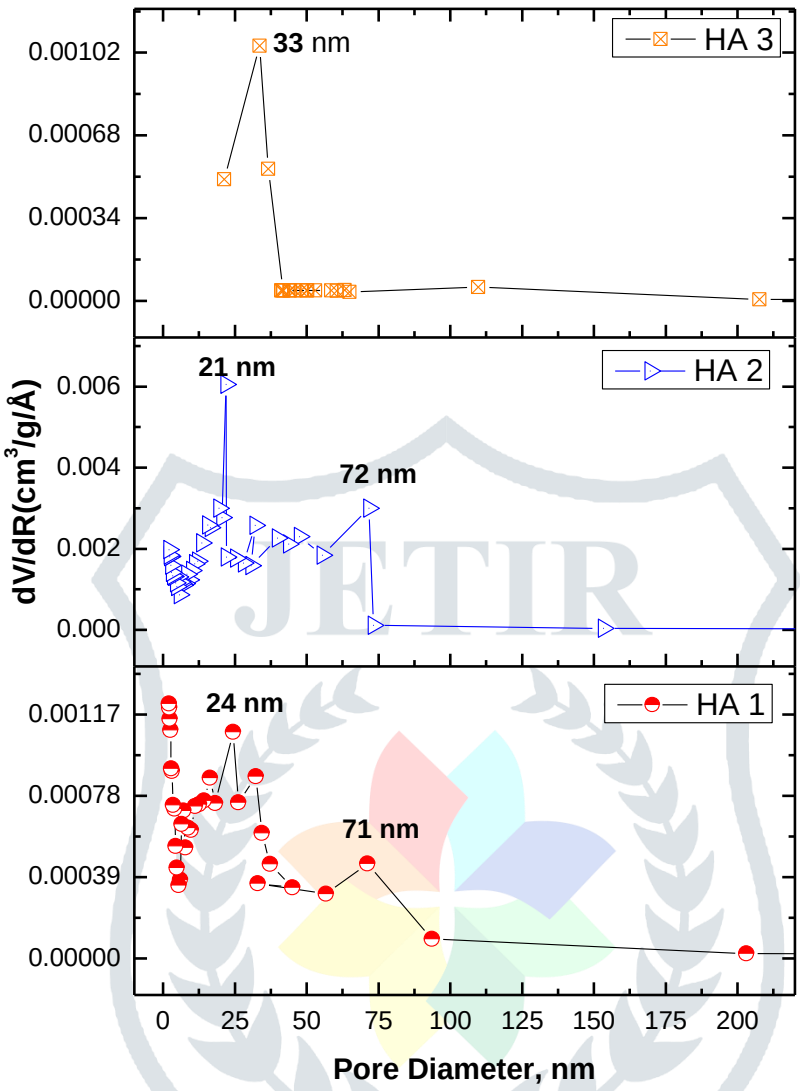

FIG. 7. BJH desportion pore size distribution of (A) HA 1, (B) HA 2 and (C) HA 3

3.3 Phase structure and composition

X-ray diffraction patterns in fig 8 shows crystal phases of as synthesized nano HA with varying surfactant ratio. All the samples synthesized had a phase pure crystalline HA structure. The predominant phase was compared with the standard JCPDS file no 09-0432 with the lattice constants a~b~0.9418 nm and c~0.6884 nm and with the P63/m space group. Even without calcination the as synthesized samples showed the hexagonal HA crystal structure[17]. At higher concentrations of surfactants, even after repeated washing, the synthesized powders were yellow in color. This was due to the traces of surfactant. Nevertheless, the crystal structure did not alter due to the presence of surfactants present in it. The peak positions and intensities matched with the calculated

intensities of P6m/3 and hence it was confirmed that the intermediates of HA like tri and bi calcium phosphates were not formed. Crystallite size of the nano HA was estimated using Scherrer's equation[18].

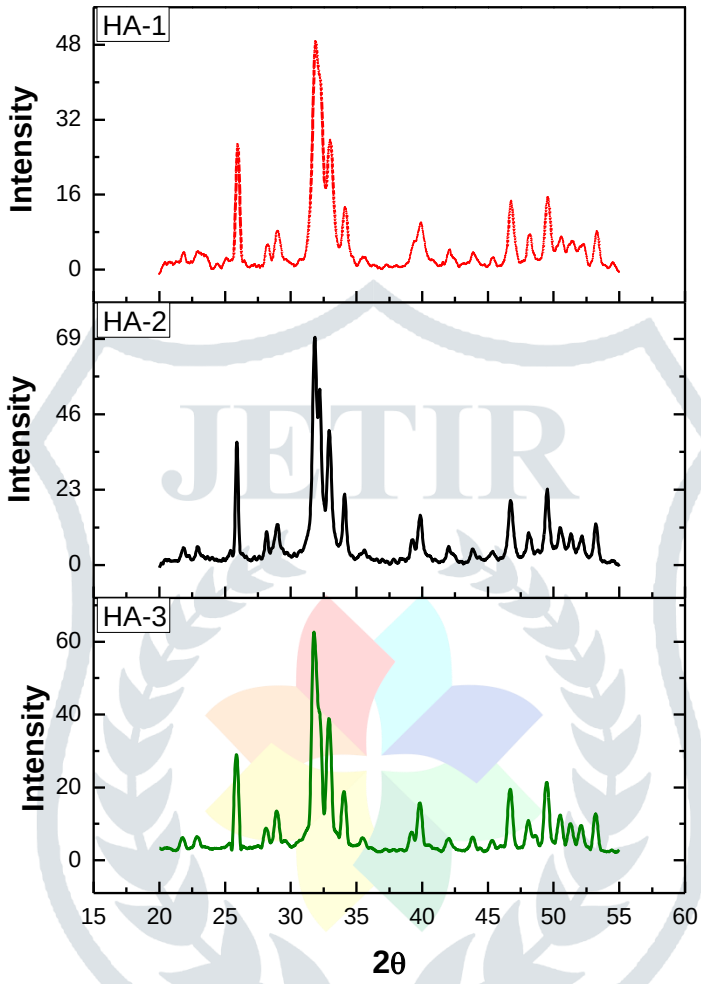

FIG. 8. X-ray patterns of hydroxyapatite synthesized using Pluronic F 127.

$$D = \frac{0.9\lambda}{\beta cos\theta} \text{.....(1)}$$

where D is the crystallite size, λ is the wave length of X-ray (0.15460 nm), β is the full-width at half maximum (radians) and θ is the diffraction angle.

Also the degree of crystallinity was evaluated by

$$X_C = \left(\frac{k}{\beta_{002}}\right)^3 \text{.....(2)}$$

where β_{002} is the full-width at half maximum of 002 reflection, k-0.24 (constant) for hydroxyapatite. Calculated degrees of crystallinities were decreasing with increase in surfactant concentration. Crystallinity of calcined sample showed slight increase in the values. It was observed that the crystallite size increased with the increase in surfactant concentration. Highest crystallite size of 49 nm was found for HA 1 and lowest crystallite size of 20 nm was observed

for the HA 3. Also it is observed that there is slight increase in peak broadness for low surfactant concentration and it starts to sharpen at higher concentration (Fig.9)

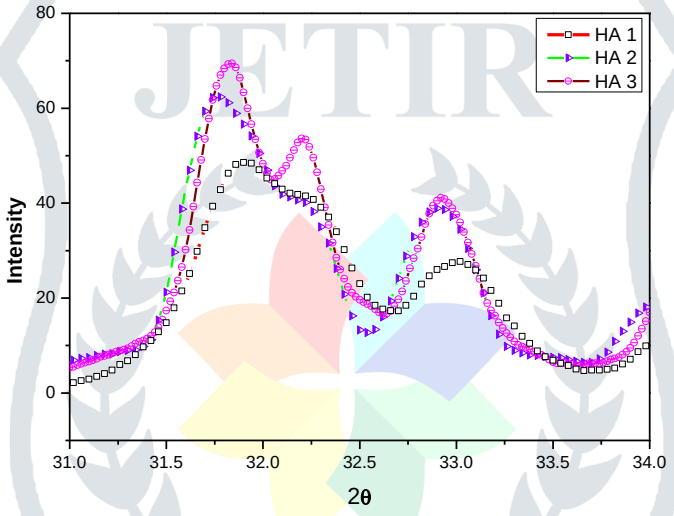

FIG. 9. X-ray patterns of hydroxyapatite synthesized using Pluronic F127, peak broadening observed in HA 1 which has higher crystallite size. (A) HA 1, (B) HA 2 and (C) HA 3

Samples obtained after synthesis were calcined at different temperatures. FTIR results of the calcined samples showed major absorption band of PO_4^{3-} stretching, which appeared at 1019 cm^{-1} in HA spectrum (fig 10). Additionally, bands at 3080cm^{-1} was observed and was assigned to CO_3^-. It is of interest to note here that the absorption bands associated with H_2O molecules distinctly appeared at 3576 cm^{-1} and 1639 cm^{-1} in the spectrum of HA. The former band at 3576 cm^{-1} was identified as the loosely physisorbed water at the surface of HA nanorods, whereas the latter arose from the chemisorbed molecular water within the HA lattice. Bands of CO_3^- was predominant even after heating at 80°C. With higher calcination temperatures, total intensity of these bands decreased for the samples at 650°C and 900°C. This confirms the elimination of CO_3^- ions at higher

temperatures. Also, bands at 630 cm^{-1} assigned to OH^- ion was not clearly visible for the sample heated at 80°C. Other absorption bands at 1040, 1093 and 962 and 571 cm^{-1} detected in the spectra are attributed to PO_4^{2-} ion.

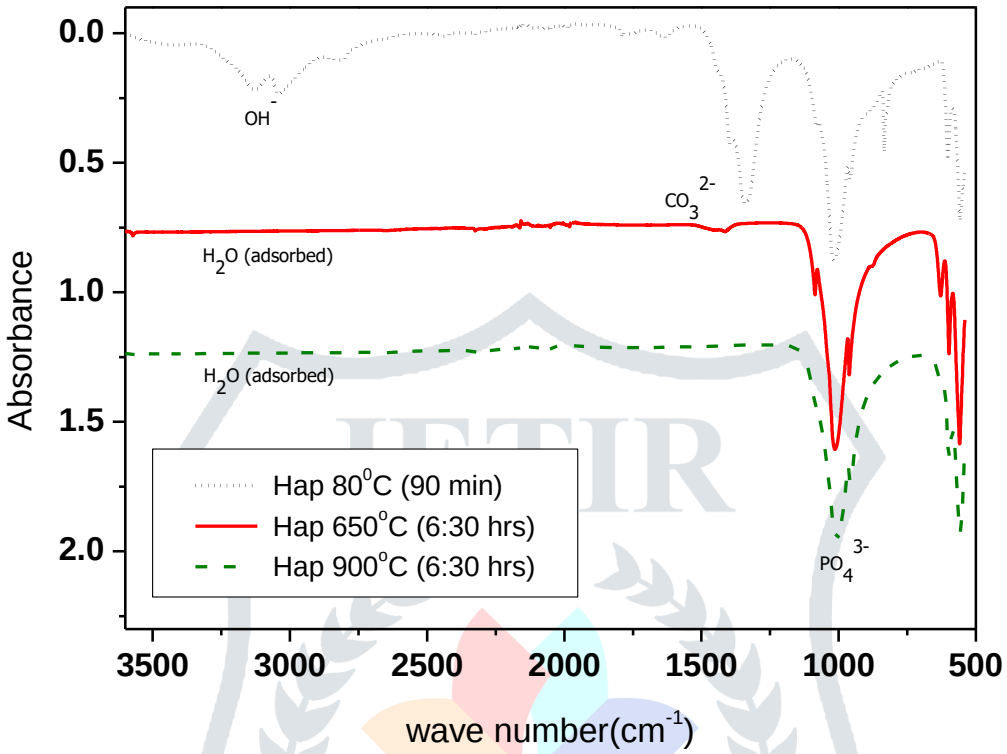

FIG. 10. FTIR spectra of sample HA 2 calcined at temperatures of 80°C. 650°C and 900°C

3.4 Mechanism of Spherical and Rod like transition

As PEO and PPO are water soluble systems, they show a varied response dependent on concentration, pressure and temperature. These fluctuations can help in tailoring the geometry of the nanoparticles by controlling the micelle geometry.

At low temperatures both PEO and PPO are hydrophilic. They behave as independent polymer chain. At temperature greater than 15°C, F127 shows an amphiphilic nature. At concentrations lower than 20wt% and at temperature lower than 15°C, spherical micelles are formed. The

transition from spherical to rod like takes place with increase in temperature and at same concentration. With this narrow temperature range, spherical micelles change via prolate ellipsoids to worm or rod like. For 6wt% concentration of F127, the transition took at around 80°C. The sphere to rod like transition reported earlier with

F127 and F88 was around T≈ 95°C [19, 20]. In our case, for 6wt% concentration the transition temperature is reduced.

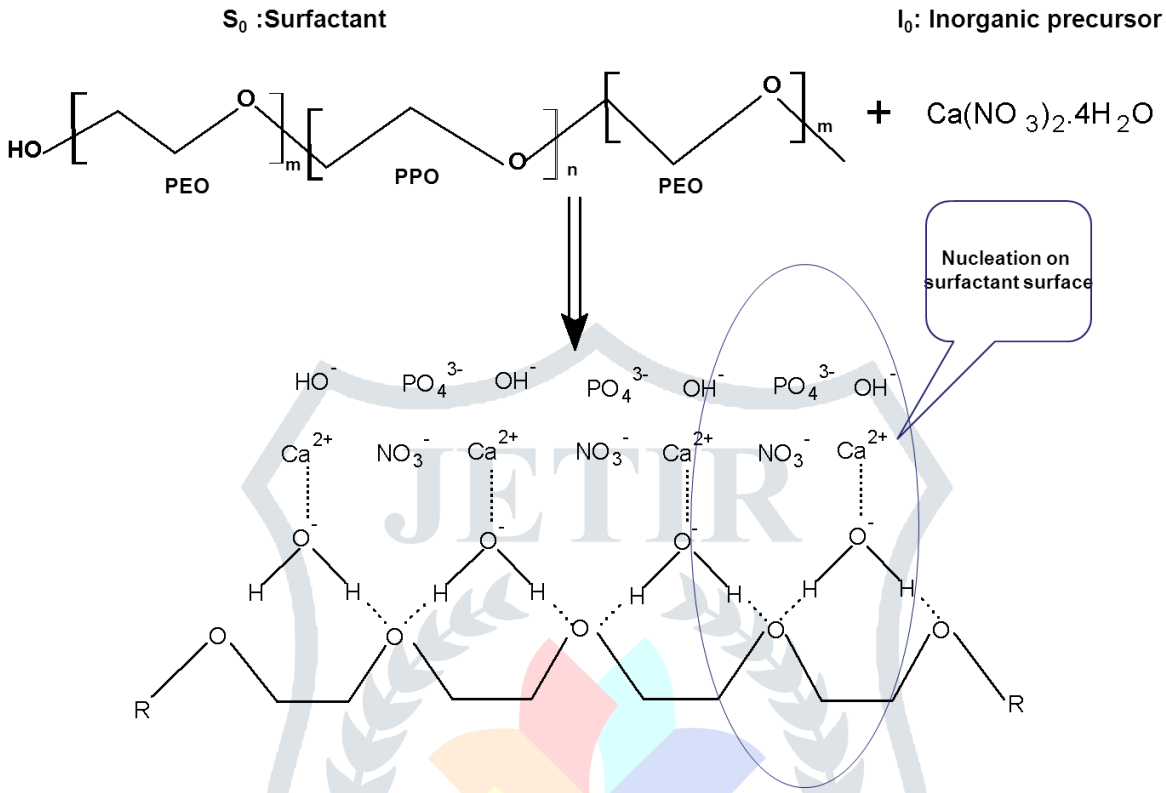

FIG. 11. Illustration of interaction process between surfactant and inorganic complex

The mesostructure formation is believed to form by the exchange reaction of ions. However, the electrostatics forces are the plausible route for initiating ionic templating. The electrostatic effects could not explain the aggregation of pluronic block copolymer and hence some other types of attraction forces may be responsible. Three ways of interaction have been schematized $(S^oH^+)(X^-I^o)$, S^oI^o and $(S^oM^+)(X^-I^o)$[21]. The S^oI^o model is highly suitable to explain our findings by hydrogen bonding between the copolymer and the inorganic complex. Block polymer in water forms micelles through the process of self aggregation. Due to different hydrophilicity and hydrophobicity they arrange in a specific manner. Ethylene oxide block being very hydrophilic will tend to form the corona in the vicinity of water molecule, whereas propylene oxide block being hydrophobic will arrange in the reverse order than EO and forms a core. As the concentration of F127 is changed, the shape of micelle will also change. This is also observed our samples where HA 1, HA2 and HA 3 has needle shaped particles and HA 4 has spherical particles. These micelles with different geometries acts as microreactors will

assist in forming the HA during crystallization and precipitation process. Calcium precursor is bonded with EO via hydrogen bonding and phosphate ions from H_3PO_4 will react with calcium ions to form hydroxyapatite. This interaction is schematically illustrated in both fig 11 and 12. The final geometry of HA depends on the micelle geometry in solution.

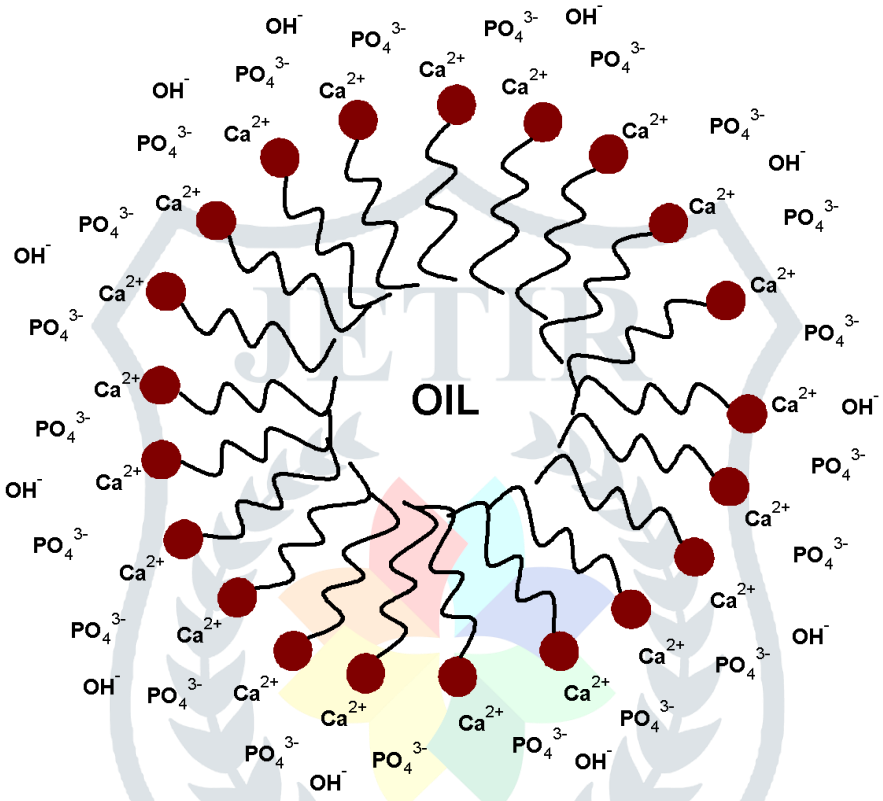

FIG. 12. Schematic representation of a micelle bonded with inorganic complex

3.5 Effect of SBF on nanoparticles

SEM micrographs of HA in Fig 13 shows the morphologies of HA before and after soaking in simulated body fluid (SBF). After one hour of soaking, precipitated particles could be observed on HA surface. These particles were similar to that of rod like numerous tiny granular apatite particles which grew on the surface. Such crystals would be expected to grow and form a layer of calcium phosphate (Ca-P) on the surface that could later crystallize to a bone like apatite crystals. The nucleation of these precipitated crystals prefer to occur in pores rather than on smooth surfaces, where the size of the precipitates is, obviously, much larger than that on the smooth part of the surfaces. As the synthesized HA nanoparticles had uniform nanopores on its surface (pore size distribution), it mediated the precipitation of apatite layer. The quantity and size of these precipitates

increased as the soaking time increased. With further increase in the soaking time, there is no significant change in the surface morphology, and small crystallites can be observed.

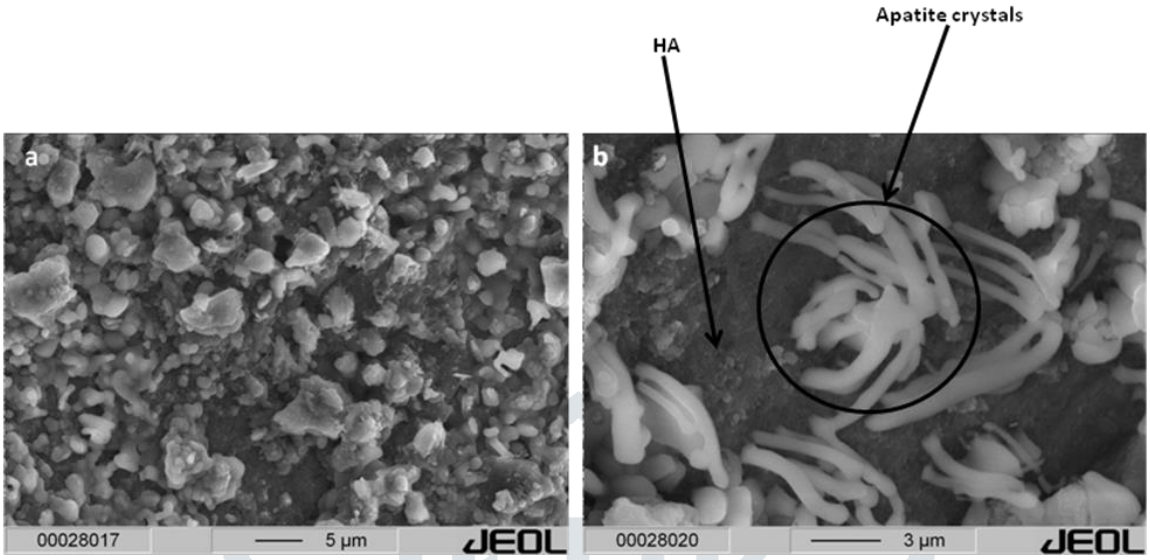

FIG. 13. SEM micrograph of Hydroxyapatite powder. a) Green powder of HA & b) After soaking in SBF solution for 2 days some areas are already covered by inorganic crystals of apatite high lightened in black circle.

EDS analysis of the HA precipitated apatite layer had the peaks of calcium, phosphorus, sodium, chlorine, carbon and oxygen. The presence of Na and Cl in the EDS spectra is attributed to residual element from the SBF solution. The thickness of apatite crystals formed on the HA surface was examined by SEM. It was found that there was no uniform layer of apatite developed on the HA, instead crystals in the form of rods sprouted from the surface randomly. Formation of apatite layer is also strongly attributed to the time of soaking. Larger soaking time results in uniform deposition. As in the case observed above, the soaking time was only limited to one day. By morphological analysis it can be confirmed that the extra structure on HA surface is by apatite layer and its existence is also confirmed by the presence of carbon in EDX analysis which also implies that the HA promotes the carbonate apatite layer formation.

3.6 Electrospinning

The morphology of electrospun pure PHB/HA nanofiber composites shown in Figure 14. The as-spun PHB nanofiber has a uniform morphology without any beads formation. In addition, the electrospun nanocomposite PHB/ nano HA rod fibers have morphology identical to those from unfilled PHB nanofibers in terms of diameter of nanofibers itself. But there was minor increase in the average fiber size due to addition of HA nanorods. Whereas the nanofibers with spherical nanoparticles showed increase in nanofiber diameter. This is

due to the bigger particle size which will eventually stretch the fiber during spinning. Nevertheless, the average fiber diameter in both the cases where below 400 nm. The typical internal morphology of the electrospun PHB containing nanoHA revealed that the HA nanoparticles are well distributed within the electrospun fibers, and it is of interest that a large number of HA nanoparticles were preferentially oriented parallel to the longitudinal direction of the electrospun PHB. Such type of orientation can facilitate the fabrication of nanofiber nanocomposites with enhanced mechanical properties. Aslo, this method is suitable to mimic the extracellular structure that is found in organic matrix fibers in the natural bone tissues having diameters in the range from 100 to 450 nm[22] .

Moreover, HA prepared with nonionic surfactant F127 can only be completely removed only after calcination at higher temperature. Nevertheless, calcining the inorganic fillers can cause agglomeration. As synthesized nanofillers when blended with polymer will have traces of nonionic surfactant layer around the fillers. Such a layer will help in improving the interfacial strength of HA based polymer nanocomposites[23, 24].

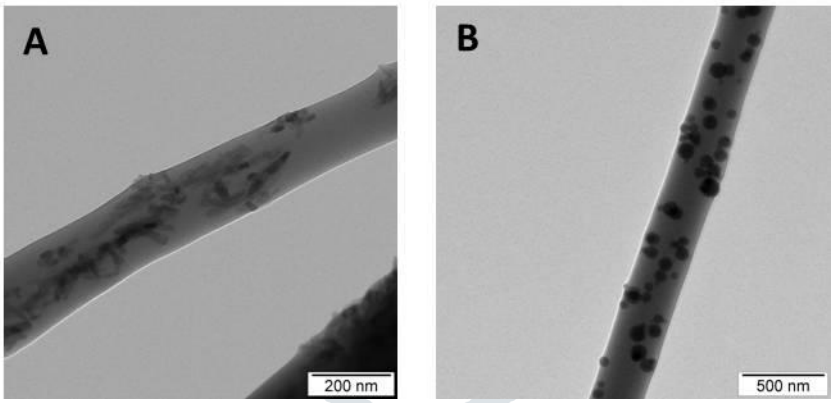

FIG. 14. TEM micrographs of electrospun PHB/HA nanofiber nanocomposites. A) PHB/HA nanorods and B) PHB/HA nano spherical.

4. Conclusions

A novel method to synthesize and control HA nanoparticle geometry was established. Pluronics templates are the best source to control the geometry of the nanoparticles which are water soluble systems and reduce the time for separating the nanoparticles. Low temperature synthesis resulted in spherical geometry and higher temperature yielded rod like geometry. Also, the porosity of nanoparticles could be controlled by adjusting the concentration of surfactant. Higher surfactant concentration shows unimodal pore size distribution and lowering the surfactants results in biomodal distribution. Nanosized pores obtained by this method can be used in nano

impregnation of drugs for tissue engineering applications. There was nanopores mediated the apatite layer formation when immersed in SBF solution in 24 h. It was also possible to fabricate nanocomposite nanofiber scaffolds for biological applications by using electrospinning as novel fabrication techniques. In conclusion, the most striking properties of electrospun PHB/HA biocomposite NF scaffold not only has the similar composition but has also similar hierarchical structure of extracellular matrix and mineral organization in bone at the nanoscale level. This might open up a wide variety of future applications for higher bioactive bone graft materials especially for non-load-bearing bone tissue engineering.

5. References

1. E.S. Ahn, N.J. Gleason, A. Nakahira and J.Y. Ying: Nanostructure Processing of Hydroxyapatite-based Bioceramics *Nano Letters.* **1**(3), 149 (2001).

2. T. Safronova, M. Shekhirev and V. Putlyaev: Ceramics based on calcium hydroxyapatite synthesized in the presence of PVA *Glass and Ceramics.* **64**(11), 408 (2007).

3. Q.J. He and Z.L. Huang: Controlled growth and kinetics of porous hydroxyapatite spheres by a template-directed method *Journal of Crystal Growth.* **300**(2), 460 (2007).

4. C. Durucan and P.W. Brown: α-Tricalcium phosphate hydrolysis to hydroxyapatite at and near physiological temperature *Journal of Materials Science: Materials in Medicine.* **11**(6), 365 (2000).

5. R. Rao, H. Roopa and T. Kannan: pH controlled dispersion and slip casting of Si₃N₄ in aqueous media *Bulletin of Materials Science.* **24**(1), 57 (2001).

6. S.-H. Rhee and J. Tanaka: Hydroxyapatite Coating on a Collagen Membrane by a Biomimetic Method *Journal of the American Ceramic Society.* **81**(11), 3029 (1998).

7. M.-P. Pileni: The role of soft colloidal templates in controlling the size and shape of inorganic nanocrystals *Nat Mater.* **2**(3), 145 (2003).

8. S. Bose and S.K. Saha: Synthesis and Characterization of Hydroxyapatite Nanopowders by Emulsion Technique *Chemistry of Materials.* **15**(23), 4464 (2003).

9. K. Mortensen: Structural studies of aqueous solutions of PEO - PPO - PEO triblock copolymers, their micellar aggregates and mesophases; a small-angle neutron scattering study *Journal of Physics: Condensed Matter*. **8**(25A), A103 (1996).

10. A. Frenot and I.S. Chronakis: Polymer nanofibers assembled by electrospinning *Current Opinion in Colloid & Interface Science.* **8**(1), 64 (2003).

11. R.L. Cook, H.E. King, Jr. and D.G. Peiffer: Pressure-induced crossover from good to poor solvent behavior for polyethylene oxide in water *Physical Review Letters.* **69**(21), 3072 (1992).

12. H.S. Liu, T.S. Chin, L.S. Lai, S.Y. Chiu, K.H. Chung, C.S. Chang and M.T. Lui: Hydroxyapatite synthesized by a simplified hydrothermal method *Ceramics International.* **23**(1), 19 (1997).

13. S. Padilla, I. Izquierdo-Barba and M. Vallet-Regí: High Specific Surface Area in Nanometric Carbonated Hydroxyapatite *Chemistry of Materials.* **20**(19), 5942 (2008).

14. M. Jaroniec and L.A. Solovyov: Improvement of the Kruk−Jaroniec−Sayari Method for Pore Size Analysis of Ordered Silicas with Cylindrical Mesopores *Langmuir.* **22**(16), 6757 (2006).

15. M. Kruk and M. Jaroniec: Gas Adsorption Characterization of Ordered Organic−Inorganic Nanocomposite Materials *Chemistry of Materials.* **13**(10), 3169 (2001).

16. H.C. Shum, A. Bandyopadhyay, S. Bose and D.A. Weitz: Double Emulsion Droplets as Microreactors for Synthesis of Mesoporous Hydroxyapatite *Chemistry of Materials.* **21**(22), 5548 (2009).

17. N. Puvvada, P.K. Panigrahi and A. Pathak: Room temperature synthesis of highly hemocompatible hydroxyapatite, study of their physical properties and spectroscopic correlation of particle size *Nanoscale.* **2**(12), 2631 (2010).

18. A.L. Patterson: The Scherrer Formula for X-Ray Particle Size Determination *Physical Review.* **56**(10), 978 (1939).

19. K. Mortensen and Y. Talmon: Cryo-TEM and SANS Microstructural Study of Pluronic Polymer Solutions *Macromolecules.* **28**(26), 8829 (1995).

20. K. Mortensen and W. Brown: Poly(ethylene oxide)-poly(propylene oxide)-poly(ethylene oxide) triblock copolymers in aqueous solution. The influence of relative block size *Macromolecules.* **26**(16), 4128 (1993).

21. Y.F. Zhao and J. Ma: Triblock co-polymer templating synthesis of mesostructured hydroxyapatite *Microporous and Mesoporous Materials.* **87**(2), 110 (2005).

22. Z. Hongpeng, N. Jun, S. Junfeng, G. Shuang and Y. Dongzhi: Electrospun chitosan/poly(vinyl alcohol) blend ultrafine fibers and their ultraviolet photocrosslinking. *Acta Polymerica Sinica.* **1**(3), 230 (2007).

23. M. Wang and W. Bonfield: Chemically coupled hydroxyapatite–polyethylene composites: structure and properties *Biomaterials.* **22**(11), 1311 (2001).

24. Y. Li, D. Li and Z. Xu: Synthesis of hydroxyapatite nanorods assisted by Pluronics *Journal of Materials Science.* **44**(5), 1258 (2009).